Monthly Notices of the ROYAL ASTRONOMICAL SOCIETY

MNRAS **497,** 1348–1364 (2020) doi:10.1093/mnras/staa1841
Advance Access publication 2020 June 26

High-sensitivity observations of molecular lines with the Arecibo Telescope

W. S. Tan,[1]★ E. D. Araya,[1]★ L. E. Lee,[1]† P. Hofner,[2]‡ S. Kurtz,[3] H. Linz[4] and L. Olmi.[5]

[1]*Physics Department, Western Illinois University, 1 University Circle, Macomb, IL 61455, USA*
[2]*Physics Department, New Mexico Institute of Mining and Technology, 801 Leroy Place, Socorro, NM 87801, USA*
[3]*Instituto de Radioastronomía y Astrofísica, Universidad Nacional Autónoma de México, Apdo. Postal 3-72, 58089, Morelia, Michoacán, Mexico*
[4]*Max Planck Institute for Astronomy, Königstuhl 17, D-69117 Heidelberg, Germany*
[5]*INAF, Osservatorio Astrofisico di Arcetri, Largo E. Fermi 5, I-50125 Firenze, Italy*

Accepted 2020 June 18. Received 2020 June 16; in original form 2019 September 12

ABSTRACT

We report on one of the highest sensitivity surveys for molecular lines in the frequency range 6.0–7.4 GHz conducted to date. The observations were done with the 305- m Arecibo Telescope toward a sample of 12 intermediate-/high-mass star-forming regions. We searched for a large number of transitions of different molecules, including CH_3OH and OH. The low rms noise of our data ($\sim$5 mJy for most sources and transitions) allowed detection of spectral features that have not been seen in previous lower sensitivity observations of the sources, such as detection of excited OH and 6.7 GHz CH_3OH absorption. A review of 6.7 GHz CH_3OH detections indicates an association between absorption and radio continuum sources in high-mass star-forming regions, although selection biases in targeted projects and low sensitivity of blind surveys imply incompleteness. Absorption of excited OH transitions was also detected toward three sources. In particular, we confirm a broad 6.035 GHz OH absorption feature in G34.26+0.15 characterized by an asymmetric blueshifted wing indicative of expansion, perhaps a large-scale outflow in this H II region.

Key words: masers – H II regions – ISM: molecules – radio lines: ISM.

1 INTRODUCTION

In the past two decades, high-sensitivity receivers have been deployed in major observatories around the world for observations at 6 GHz frequencies. Different molecular transitions have been detected at these frequencies, particularly in regions of high-mass star formation. The main examples are excited OH transitions (e.g. Al-Marzouk et al. 2012; Avison et al. 2016) and the widespread 6.7 GHz methanol line.

The 6.7 GHz methanol transition was first detected in the interstellar medium by Menten (1991) using the 140-foot telescope of the NRAO (National Radio Astronomy Observatory). Menten (1991) detected strong methanol masers associated with star-forming regions, as well as methanol absorption toward eight regions (NGC 2264, G345.70–0.09, NGC 6334−C, Sgr A−F, Sgr A−A, Sgr B2, G10.62–0.38, and W33). Since then, most observations have focused on studies of the 6.7 GHz CH_3OH maser as part of blind surveys (e.g. Pandian, Goldsmith & Deshpande 2007; Breen et al. 2015), targeted observations of high-mass star-forming regions (e.g. Olmi et al. 2014), or to investigate periodic maser flares (e.g. Goedhart, Gaylard & van der Walt 2004; Araya et al. 2010; MacLeod et al. 2018; Szymczak et al. 2018; Rajabi et al. 2019). While most observations reported in the literature have focused on bright lines, high-sensitivity observations have resulted in detection of weak lines, such as 6.7 GHz methanol absorption in the low-mass star-forming region NGC 1333 (Pandian et al. 2008). In this case, the line is due to an anti-inversion (overcooling) effect that allows absorption against the cosmic microwave background (CMB), as observed for example in 6 cm H_2CO (e.g. Araya et al. 2006) and 12 GHz CH_3OH transitions (Walmsley et al. 1988; Peng & Whiteoak 1991). Pandian et al. (2008) concluded that the methanol absorption in NGC 1333 is tracing dense ($\sim 10^6$ cm^{-3}) cold/warm ($\sim$15 to 30 K) gas.

In extragalactic environments, high-sensitivity observations have shown that 6.7 GHz methanol absorption is rare (Ellingsen et al. 1994), for example it was not detected in the Karl G. Jansky Very Large Array (VLA) observations of M31 by Sjouwerman et al. (2010). Extragalactic 6.7 GHz methanol absorption has only been reported towards the nucleus of the active galaxy NGC 3079 (Impellizzeri et al. 2008), the ultraluminous infrared (IR) galaxy Arp 220 (Salter et al. 2008), and a tentative detection toward Mrk 348 (Impellizzeri 2008).

Previous high-sensitivity and high-spectral resolution observations of CH_3OH and other molecular species have shown the potential of high-sensitivity studies for detection of weak variable masers, narrow lines tracing quiescent molecular clouds, and absorption features with high-velocity linewidths that could trace outflows (e.g. Araya et al. 2006; Al-Marzouk et al. 2012). Indeed, a great analytic potential is open when lines are found in absorption against contin-

★ E-mail: ws-tan@wiu.edu (WST); ed-araya@wiu.edu (EDA)
† Present address: Department of Physics and Astronomy, University of Missouri, Columbia, MO 65211, USA.
‡ Adjunct Astronomer at the National Radio Astronomy Observatory, 1003 Lopezville Road, Socorro, NM 87801, USA.

Table 1. Source list.

Source	l (°)	b (°)	RA (J2000) (h m s)	Dec. (J2000) (° ′ ″)	Configuration
IRAS 18472 − 0022[a]	32.466	0.209	18 49 50.70	−00 19 09.0	1
G34.26+0.15	34.257	0.154	18 53 18.50	+01 14 59.0	1,2
IRAS 18517+0437	37.427	1.518	18 54 13.80	+04 41 32.0	1
IRAS 18566+0408	37.554	0.201	18 59 09.98	+04 12 15.6	2
IRAS 19012+0536	39.387	− 0.140	19 03 45.10	+05 40 40.0	1
G45.07+0.13	45.071	0.132	19 13 22.10	+10 50 53.0	1
G45.12+0.13	45.122	0.133	19 13 27.80	+10 53 37.0	1,2
G45.47+0.05	45.466	0.046	19 14 25.60	+11 09 26.0	1
IRAS 19266+1745[a]	53.032	0.117	19 28 54.00	+17 51 56.0	1
IRAS 20051+3435	71.892	1.312	20 07 03.80	+34 44 35.0	1
G69.54–0.98	69.540	− 0.976	20 10 09.10	+31 31 34.3	2
IRAS 20081+2720[a]	66.153	− 3.185	20 10 11.50	+27 29 06.0	1

Notes. Two different spectrometer configurations were used in the main survey to observe different molecular transitions (see Table 2).
[a]Observations were conducted toward IRAS coordinates (Sridharan et al. 2002), which differ by ∼30–55 arcsec with respect to the location of 1.2 mm sources (Beuther et al. 2002), thus, the observations may be affected by pointing offsets.

Table 2. Spectral lines observed in the main survey.

Species	Rest frequency (MHz)	E_u/k_B (K)	Channel width (km s^{-1})	Detection[a]	Configuration[b]
CH	7275.0040	96.7	0.13	N	2
CH	7325.2030	96.7	0.13	N	2
CH	7348.4190	96.7	0.06	E?	2
CH	7398.6180	96.7	0.12	N	2
CH_3CHO	6389.9330	8.0	0.14	N	1
CH_3C_5N	6224.3425	8.3	0.15	N	1
CH_3OH	6668.5192	49.1	0.07	E, A	1,2
CH_3OH	6744.8430	803.7	0.14	N	2
CH_3OH	6853.6870	353.5	0.07	E?	2
CH_3OH	7283.4490	215.9	0.06	E?	2
D_2CO	6096.0682	8.4	0.15	N	1
H_2CS	6278.6500	23.2	0.15	A	1
H99α	6676.0750	RRL	0.34	E	1
OH	6035.0932	120.8	0.08	E, A	1

Notes. Spectroscopic information is from Splatalogue (http://www.cv.nrao.edu/php/splat/).
[a](E) emission; (A) absorption; (N) non-detection; (?) tentative detection (we report tentative detections only toward IRAS 18566+0408). The tentative detections were not confirmed in our follow-up observations (Table 3), thus it is unclear whether the lines are variable masers or artefacts.
[b]The transitions corresponding to Configuration 1 were observed on 2008 October 13 and 14. The Configuration 2 transitions were observed on 2008 October 27.

uum provided by target sources. Combined with high-sensitivity and good velocity resolution, the kinematics of the gas along the line of sight to the targets can be probed, and the absorption nature removes a geometric ambiguity regarding the interpretation.

Motivated by the potential of high-sensitivity and high-spectral resolution studies, we conducted observations of a sample of 12 intermediate- and high-mass star-forming regions with the 305- m Arecibo Telescope in Puerto Rico. Our observations were carried out in two main runs as described in Section 2. Results and discussion are presented in Sections 3 and 4, respectively, where we focus on 6.7 GHz CH_3OH absorption and excited OH lines. Our conclusions are given in Section 5.[1]

[1]This work is based on the MS thesis 'Survey for C-Band High Spectral Lines with the Arecibo Telescope', by Tan (2017).

2 OBSERVATIONS AND DATA REDUCTION

2.1 Main survey

The 305- m Arecibo Telescope in Puerto Rico was used to observe 12 intermediate- and high-mass star-forming regions in the first Galactic quadrant (Table 1). The sources were mostly selected from two main samples: high-mass protostellar candidates from Sridharan et al. (2002), which were observed by Araya et al. (2004), and regions known to harbour ultracompact (UC) H II regions and prominent hot molecular cores (Wood & Churchwell 1989; Kurtz et al. 2000), that is regions similar to G31.41+0.31 (e.g. Araya et al. 2008). Specifically, six sources (IRAS 18472−0022, G34.26+0.15, G45.07+0.13, G45.12+0.13, G45.47+0.05, and G69.54–0.98) have been classified as UCHII regions (Wood & Churchwell 1989; Kurtz, Churchwell & Wood 1994; Hoare et al. 2012; Purcell et al. 2013), four sources

Table 3. Follow-up observations.

Species	Rest frequency (MHz)	E_u/k_B (K)	IRAS 18566+0408			G45.12+0.13		
			Rms (mJy)	Channel width (km s^{-1})	Detection[a]	Rms (mJy)	Channel width (km s^{-1})	Detection[a]
CH	7275.0040	96.7	3.1	0.16	N	18	0.16	N
CH	7325.2030	96.7	RFI	–	–	RFI	–	–
CH	7348.4190	96.7	3.6	0.16	**N**	18	0.16	N
CH	7398.6180	96.7	3.1	0.15	N[b]	18	0.15	N
CH_3OH	6668.5192	49.1	4.9	0.03	E	4.9	0.10	E, A
CH_3OH	6744.8430	803.7	3.0	0.17	N	16	0.17	N
CH_3OH	6853.6870	353.5	2.4	0.17	**N**	15	0.17	N
CH_3OH	7283.4490	215.9	3.2	0.16	**N**	17	0.15	N
H99α	6676.0750	RRL	4.5	0.17	N	3.0	0.51	E
H_2CS	6278.6500	23.2	4.4	0.18	N	4.7	0.18	N
OH	6016.7460	120.8	5.2	0.19	N	3.3	0.38	A
OH	6030.7485	120.8	4.5	0.19	N	7.1	0.08	E, A
OH	6035.0932	120.8	4.6	0.19	E	6.7	0.08	E, A
OH	6049.0840	120.8	3.5	0.38	N[b]	5.4	0.19	N

Notes. Radio continuum was not measured because the observations were conducted in total power ON-source mode. Spectroscopic information is from Splatalogue (http://www.cv.nrao.edu/php/splat/).
[a](–) spectral window corrupted by RFI; (E) emission; (A) absorption; (N) non-detection. We highlight with boldface (**N**) transitions that were tentatively detected in the main survey (Table 2) but not detected in the follow-up observations.
[b]Two narrow variable lines at 96.2 and 98.3 km s^{-1} were detected in most IRAS 18566+0408 7.398 GHz CH scans, most likely caused by low-level RFI. A weak (∼10 mJy) 6.049 GHz OH feature at 60 km s^{-1} was also detected toward IRAS 18566+0408, but it is most likely a bandpass artefact.

Table 4. Detection summary.

Source	OH			H_2CS	CH_3OH		CH	H99α
	6.016 GHz	6.031 GHz	6.035 GHz	6.279 GHz	6.668 GHz	7.283 GHz	7.348 GHz	6.676 GHz
IRAS 18472−0022	...	...	N	N	N	...	...	N
G34.26+0.15	...	...	E,A	A	E,A	N	N	E
IRAS 18517+0437	...	...	N	N	E	...	...	N
IRAS 18566+0408	N	N	E	N	E	E?	E?	N
IRAS 19012+0536	...	...	N	N	E	...	...	N
G45.07+0.13	...	...	E,A	N	E	...	...	E
G45.12+0.13	A	E,A	E,A	N	E?,A	N	N	E
G45.47+0.05	...	...	E	N	E,A	...	...	E
IRAS 19266+1745	...	...	N	N	E	...	...	N
IRAS 20051+3435	...	...	N	N	N	...	...	N
G69.54–0.98	...	...	...	...	E,A	N	N	...
IRAS 20081+2720	...	...	N	N	N	...	...	N

Notes. Summary of transitions with at least one detection. (E) emission; (A) absorption; (N) non-detection; (...) not observed; and (?) tentative detection.

(IRAS 18517+0437, IRAS 18566+0408, IRAS 19012+0536, and IRAS 19266+1745) are characterized by weak radio continuum emission at few mJy to sub-mJy levels (Rosero et al. 2016), and two sources (IRAS 20051+3435 and IRAS 20081+2720) have 3.6 cm flux density upper limits of 100 mJy from Sridharan et al. (2002) and may be intermediate-mass star-forming regions based on their FIR luminosity (2×10^2 or 10^4 $L_\odot$ for IRAS 20051+3435 depending on kinematic distance and 3×10^2 $L_\odot$ for IRAS 20081+2720, Sridharan et al. 2002). No homogeneous mass determination is available for all sources in our sample, however, gas masses (estimated from dust continuum and/or molecular gas observations, Miralles, Rodriguez & Scalise 1994; Beuther et al. 2002; Williams, Fuller & Sridharan 2004; Cesaroni et al. 2015) are above ∼600 $M_\odot$ for all but two sources: IRAS 20051+3435 (95 or 510 $M_\odot$ depending on kinematic distance, Beuther et al. 2002) and IRAS 20081+2720 (∼10 $M_\odot$, Beuther et al. 2002).

We used the C-Band High receiver and the Wideband Arecibo Pulsar Processor (WAPP) spectrometer to observe 13 molecular transitions and one radio recombination line in two different configurations, each one with its own set of spectral windows. Configuration 1 was observed on 2008 October 13 and 14. Configuration 2 was observed on 2008 October 27. Table 2 lists the specific spectral lines (grouped by molecule), upper energy level of the transitions, final channel width after smoothing (smaller channel widths were used in the case of narrow lines, including tentative detections), whether a spectral line was detected, and the configuration. All spectral windows were observed with a bandwidth of 3.125 MHz (corresponding to velocity ranges between 125 and 155 km s^{-1} at the observed frequencies), 9 level sampling, dual linear polarization, and 2048 channels (1.5 kHz initial channel spacing). The sources were observed in ON-OFF (position-switched mode) with 5 min integration ON-source per scan; two scans were obtained per source in most cases. All data reduction was done in IDL[2] using the Arecibo Observatory (AOIDL) routines.

[2]IDL (Interactive Data Language) is a trademark of Harris Geospatial Corp.

Table 5. 6.7 GHz CH_3OH line parameters.

Source	$S_{\nu,\,\mathrm{cont}}$ (Jy)	Rms (mJy)	S_ν (Jy)	V_{LSR} ($\mathrm{km\,s^{-1}}$)	Width ($\mathrm{km\,s^{-1}}$)	$\int S_\nu \mathrm{d}v$ ($\mathrm{Jy\,km\,s^{-1}}$)
G34.26+0.15	4.0	6.8	0.105	55.29(0.07)	1.0(0.1)	0.063
	4.0	6.8	1.42	56.80(0.07)	1.5(0.1)	0.835
	4.0	6.8	22.9	57.69(0.07)	0.7(0.1)	8.85
	4.0	6.8	22.0	57.90(0.07)	1.0(0.1)	7.71
	4.0	6.8	0.148	59.61(0.07)	0.7(0.1)	0.067
	4.0	6.8	2.04	60.64(0.07)	0.7(0.1)	0.738
	4.0	6.8	1.51	61.19(0.07)	0.4(0.1)	0.458
	4.0	6.8	0.664	61.60(0.07)	0.6(0.1)	0.197
	4.0	6.8	−0.318	62.06(0.07)	[3.1, 5.8][a]	...
IRAS 18517+0437	<0.1	3.2	212	41.22(0.07)	2.6(0.1)	126
	<0.1	3.2	0.239	42.80(0.07)	0.8(0.1)	0.118
	<0.1	3.2	2.03	45.20(0.07)	2.1(0.1)	1.89
	<0.1	3.2	2.93	46.02(0.07)	1.6(0.1)	1.44
	<0.1	3.2	0.164	47.64(0.07)	0.6(0.1)	0.084
	<0.1	3.2	0.380	48.39(0.07)	1.0(0.1)	0.209
	<0.1	3.2	0.507	49.32(0.07)	0.8(0.1)	0.204
	<0.1	3.2	0.140	49.91(0.07)	1.1(0.1)	0.124
	<0.1	3.2	1.34	51.44(0.07)	1.2(0.1)	0.627
IRAS 18566+0408	<0.1	4.5	0.367	78.48(0.07)	0.7(0.1)	0.139
	<0.1	4.5	2.19	79.72(0.07)	1.6(0.1)	1.43
	<0.1	4.5	4.89	83.77(0.07)	1.0(0.1)	1.87
	<0.1	4.5	2.38	84.59(0.07)	0.6(0.1)	1.29
	<0.1	4.5	3.24	84.94(0.07)	0.8(0.1)	1.41
	<0.1	4.5	0.444	85.61(0.07)	0.4(0.1)	0.181
	<0.1	4.5	2.03	86.38(0.07)	1.5(0.1)	1.30
	<0.1	4.5	0.351	87.88(0.07)	0.9(0.1)	0.187
	[b]	4.9	0.175	78.48(0.03)	0.7(0.1)	0.070
	[b]	4.9	1.55	79.71(0.03)	1.5(0.1)	1.08
	[b]	4.9	4.25	83.76(0.03)	0.9(0.1)	1.53
	[b]	4.9	2.04	84.58(0.03)	0.7(0.1)	0.981
	[b]	4.9	3.57	84.96(0.03)	0.6(0.1)	1.25
	[b]	4.9	0.567	85.61(0.03)	0.6(0.1)	0.228
	[b]	4.9	1.78	86.40(0.03)	1.1(0.1)	1.02
	[b]	4.9	0.556	87.84(0.03)	0.8(0.1)	0.216
IRAS 19012+0536	<0.1	3.4	0.410	58.52(0.07)	0.7(0.1)	0.185
	<0.1	3.4	0.542	58.92(0.07)	0.6(0.1)	0.236
	<0.1	3.4	0.253	59.61(0.07)	0.5(0.1)	0.129
	<0.1	3.4	1.16	60.43(0.07)	1.3(0.1)	0.662
	<0.1	3.4	0.026	61.19(0.07)	0.3(0.1)	0.008
	<0.1	3.4	0.286	61.61(0.07)	0.9(0.1)	0.113
	<0.1	3.4	0.049	62.36(0.07)	0.3(0.1)	0.020
	<0.1	3.4	0.108	62.98(0.07)	0.8(0.1)	0.059
	<0.1	3.4	0.038	63.46(0.07)	0.5(0.1)	0.016
	<0.1	3.4	0.078	64.76(0.07)	0.8(0.1)	0.042
	<0.1	3.4	0.052	65.45(0.07)	0.6(0.1)	0.024
	<0.1	3.4	0.032	66.00(0.07)	0.4(0.1)	0.013
	<0.1	3.4	0.032	66.41(0.07)	0.9(0.1)	0.016
	<0.1	3.4	0.448	68.60(0.07)	1.1(0.1)	0.311
	<0.1	3.4	0.321	69.43(0.07)	0.7(0.1)	0.193
	<0.1	3.4	0.216	69.84(0.07)	0.4(0.1)	0.071
	<0.1	3.4	0.057	70.26(0.07)	0.3(0.1)	0.018
	<0.1	3.4	0.058	70.63(0.07)	0.6(0.1)	0.027
	<0.1	3.4	0.054	71.83(0.07)	0.9(0.1)	0.027
	<0.1	3.4	0.020	72.79(0.07)	0.4(0.1)	0.007
	<0.1	3.4	0.053	75.47(0.07)	0.5(0.1)	0.002
G45.07+0.13	0.4	3.5	0.029	55.97(0.07)	0.5(0.1)	0.012
	0.4	3.5	41.5	57.83(0.07)	2.2(0.1)	19.3
	0.4	3.5	0.397	59.75(0.07)	0.9(0.1)	0.151
G45.12+0.13	4.1	6.3	0.063	57.89(0.07)	0.8(0.1)	0.032
[c]	4.1	6.3	−0.026	59.3(0.2)	3.3(0.3)	−0.091
[c, d]	4.9	8.0	−0.024	59.5(0.2)	3.0(0.4)	−0.078
	[b]	5.6	0.046	57.8(0.1)	0.7(0.2)	0.021
[c]	[b]	5.6	−0.024	59.6(0.1)	3.8(0.3)	−0.096

Table 5 – *continued*

Source	$S_{\nu,\,\mathrm{cont}}$ (Jy)	Rms (mJy)	S_ν (Jy)	V_{LSR} (km s^{-1})	Width (km s^{-1})	$\int S_\nu \mathrm{d}v$ (Jy km s^{-1})
G45.47+0.05	0.4	3.4	1.04	56.04(0.07)	0.8(0.1)	0.498
	0.4	3.4	0.880	56.52(0.07)	0.8(0.1)	0.477
	0.4	3.4	0.960	57.48(0.07)	0.8(0.1)	0.470
	0.4	3.4	0.860	58.17(0.07)	0.9(0.1)	0.422
	0.4	3.4	0.150	59.13(0.07)	0.7(0.1)	0.063
	0.4	3.4	0.060	59.61(0.07)	0.4(0.1)	0.019
	0.4	3.4	0.040	66.27(0.07)	2.0(0.1)	0.075
	0.4	3.4	−0.030	63.25(0.07)	3.4(0.1)	−0.056
IRAS 19266+1745	<0.1	3.6	0.930	10.14(0.07)	0.8(0.1)	0.421
G69.54–0.98	0.1	3.8	13.0	0.00(0.07)	1.2(0.1)	6.37
	0.1	3.8	2.28	1.16(0.07)	1.2(0.1)	1.19
	0.1	3.8	0.115	2.47(0.07)	0.9(0.1)	0.063
	0.1	3.8	57.1	14.68(0.07)	1.8(0.1)	20.8
	0.1	3.8	0.469	15.64(0.07)	0.5(0.1)	0.131
	0.1	3.8	−0.018	11.87(0.07)	[1.6, 5.2][a]	...

Notes. [a]A linewidth range ([minimum, maximum]) is given as overlapping maser lines preclude exact measurement. Integrated flux density could not be reliably measured because the absorption line is blended with a strong maser. The absorption was fit and removed from the spectrum to measure the line parameters of the masers.
[b]Data from 2014 March observations (see Table 3; radio continuum was not measured because the observations were conducted in total power ON-source mode).
[c]Line parameters are from a Gaussian fit, 1σ statistical errors from the fit are listed. The FWHM is listed as width.
[d]G45.12+0.13 was also observed on 2008 October 27.

The position-switched observations allowed us to correct the ON-source spectra for bandpass structures and to measure the radio continuum from the bandpass level (e.g. see Watson et al. 2003), which is reliable as long as the reference position samples a similar extended background radiation and has no compact bright continuum source. In our experience, radio continuum measurements with the Arecibo Telescope from position-switched observations are reliable above ∼100 mJy; in lines of sight with low confusion levels, reproducible continuum measurements below 100 mJy have been obtained (e.g. Strack et al. 2019).

We observed the quasars B1829+290 and B1857+129 to check the pointing performance, telescope gain, system temperature (T_{sys}) and half-power beamwidth (HPBW). At a frequency of 6600 MHz, the average system temperature was 30 K, the pointing was better than 15 arcsec (mostly better than 5 arcsec), the HPBW was ∼43 arcsec, and the gain was ∼6.0 K Jy^{-1}. We checked the OFF-source spectra to look for emission/absorption in the reference position and the dynamic spectra of the ON-source observations to identify radio frequency interference (RFI). We did not find evidence for RFI or other potential bandpass artefacts for the transitions marked as tentative detections in Table 2. The T_{sys} ×(ON-OFF)/OFF spectra (i.e. the antenna temperature) were calibrated to flux density units (Jy) using the telescope gain. After checking for consistency, the two polarization signals and different scans were averaged, and the final spectra were smoothed to measure the line parameters. The typical rms was ∼5 mJy per spectral window (∼0.1 km s^{-1} typical smoothed channel width; see Table 2).

2.2 Follow-up observations

Additional observations with the Arecibo Telescope were conducted on 2014 March 17, to re-observe two of the sources in the sample. We used the WAPP spectrometer to observe 14 different spectral lines observed in two spectrometer setups. The spectrometer setups used in the follow-up observations were different than those used in the main survey (Table 3). The first spectrometer setup was tuned to OH (6.016, 6.030, 6.035, and 6.049 GHz), H99α, 6.279 GHz H_2CS, and 6.668 GHz CH_3OH transitions; the second setup was tuned to CH_3OH (6.668, 6.744, 6.854, and 7.283 GHz) and CH (7.275, 7.325, 7.348, and 7.398 GHz) transitions. Both sets of spectral lines were observed using a 3.125 MHz bandwidth per spectral window, which is equivalent to 125–155 km s^{-1} for the frequency range of 6.0–7.4 GHz of our observations. Each spectral window had 4096 channels, with a channel separation of 0.76 kHz (31–38 m s^{-1}). The observations were done in total power ON-source mode. A diode signal was used to calibrate the data to antenna temperature, and the spectra were scaled to flux density units using the telescope gain. All calibration was done using the AOIDL routines provided by the observatory. We observed the calibrator B1857+129 for pointing and system checking. At a frequency of 6650 MHz, the pointing accuracy was better than 5 arcsec, T_{sys} = 32 K, HPBW ∼ 43 arcsec, telescope gain ∼5.6 K Jy^{-1}. After calibration, the data were exported to CLASS[3] for baseline subtraction, smoothing, and to measure line parameters. Table 3 lists the observed molecules, frequencies, rms, final channel width after smoothing, and whether a line was detected toward IRAS 18566+0408 and G45.12+0.13. Multiple scans for some configurations were obtained to reduce rms.

3 RESULTS

We report detection of 6.7 GHz CH_3OH emission toward nine regions (although the line toward G45.12+0.13 could be due to a bright maser in the sidelobe of the telescope, see below), and 6.7 GHz CH_3OH absorption toward four sources (three new detections: G45.12+0.13, G45.47+0.05, and G69.54−0.98). We also report 6.035 GHz OH emission toward five sources (G45.07+0.13 being a new detection to our knowledge); H99α emission toward four sources; and the first detection of 6.016 GHz and 6.030 GHz OH lines toward G45.12+0.13. A summary of detections and non-detections of the different spectral

[3]CLASS is part of the GILDAS software package developed by IRAM.

Table 6. Line parameters of 6.035 GHz OH.

Source	$S_{\nu,\,\mathrm{cont}}$ (Jy)	Rms (mJy)	S_ν (Jy)	V_{LSR} (km s^{-1})	Width (km s^{-1})	$\int S_\nu \mathrm{d}v$ (Jy km s^{-1})
G34.26+0.15	4.3	8.1	0.282	55.84(0.08)	1.0(0.2)	0.122
	4.3	8.1	0.027	56.90(0.08)	0.4(0.2)	0.007
	4.3	8.1	0.351	58.19(0.08)	0.8(0.2)	0.116
	4.3	8.1	0.465	58.49(0.08)	0.7(0.2)	0.163
	4.3	8.1	0.171	59.63(0.08)	0.5(0.2)	0.050
	4.3	8.1	0.062	60.24(0.08)	0.4(0.2)	0.019
	4.3	8.1	0.352	60.92(0.08)	0.9(0.2)	0.155
	4.3	8.1	0.119	62.06(0.08)	0.4(0.2)	0.030
	4.3	8.1	0.163	62.51(0.08)	0.5(0.2)	0.048
	4.3	2.9[a]	− 0.062	50.8(1.1)	[57, 80]	...
IRAS 18566+0408	[b]	4.6	0.014	85.8(0.2)	0.6(0.4)	0.007
G45.07+0.13	0.4	3.1	0.232	55.85(0.08)	0.8(0.2)	0.098
	0.4	3.1	0.128	57.59(0.08)	1.0(0.2)	0.065
	0.4	3.1	0.018	58.19(0.08)	0.5(0.2)	0.008
	0.4	3.1	0.015	60.69(0.08)	0.4(0.2)	0.007
	0.4	3.1	0.086	62.75(0.08)	0.6(0.2)	0.026
	0.4	3.1	− 0.021	50.84(0.08)	10.0(0.2)	− 0.089
G45.12+0.13	4.1[c]	5.5	− 0.024	51.8(0.3)	1.6(0.6)	− 0.041
	4.1	5.5	2.20	53.87(0.08)	0.9(0.2)	1.13
	4.1	5.5	2.54	54.32(0.08)	1.0(0.2)	1.42
	4.1	5.5	1.16	55.54(0.08)	0.8(0.2)	0.475
	4.1[c]	5.5	− 0.111	58.24(0.09)	3.3(0.2)	− 0.390
	[b, c]	7.1	− 0.035	51.9(0.3)	1.4(0.7)	− 0.051
	[b]	7.1	2.54	53.87(0.08)	1.9(0.2)	2.495
	[b]	7.1	1.75	55.49(0.08)	0.8(0.2)	0.680
	[b, c]	7.1	− 0.129	58.2(0.1)	3.5(0.4)	− 0.484
G45.47+0.05	0.5	3.7	0.018	60.09(0.08)	0.4(0.2)	0.004
	0.5	3.7	0.040	60.62(0.08)	0.3(0.2)	0.012
	0.5	3.7	0.013	61.15(0.08)	0.4(0.2)	0.004
	0.5	3.7	0.049	61.60(0.08)	0.5(0.2)	0.017
	0.5	3.7	0.033	61.91(0.08)	0.5(0.2)	0.014
	0.5	3.7	0.174	62.82(0.08)	0.7(0.2)	0.063
	0.5	3.7	0.752	63.28(0.08)	0.6(0.2)	0.323
	0.5	3.7	0.510	63.67(0.08)	0.5(0.2)	0.228
	0.5	3.7	0.902	64.41(0.08)	0.6(0.2)	0.445
	0.5	3.7	3.84	65.02(0.08)	0.8(0.2)	1.96
	0.5	3.7	3.10	65.86(0.08)	0.7(0.2)	1.66
	0.5	3.7	7.51	66.31(0.08)	1.3(0.2)	3.76
	0.5	3.7	3.21	68.14(0.08)	1.9(0.2)	2.66

Notes. [a]Spectra smoothed to a channel width of 1.1 km s^{-1} to measure the peak flux density and velocity of a weak and broad absorption line. Because of the broad asymmetric absorption profile and overlapping bright masers, a linewidth range is given ([minimum, maximum]), and the integrated flux density was not reliably measured. The absorption was fit and removed from the spectrum to measure the line parameters of the masers.
[b]Data from 2014 March observations (see Table 3; radio continuum was not measured because the observations were conducted in total power ON-source mode).
[c]Line parameters from Gaussian fit. FWHM reported as line width. Two absorption lines fitted with independent Gaussians in this spectrum, however, it is likely that the absorption is a single broad line blended with masers.

Table 7. H99α line parameters.

Source	$S_{\nu,\,\mathrm{cont}}$ (Jy)	Rms (mJy)	S_ν (Jy)	V_{LSR} (km s^{-1})	FWHM (km s^{-1})	$\int S_\nu \mathrm{d}v$ (Jy km s^{-1})
G45.07+0.13	0.4	2.2	0.012	55.5(0.5)	24.9(1.1)	0.313
G45.47+0.05	0.5	2.6	0.022	59.8(0.3)	31.7(0.7)	0.733

Notes. Line parameters obtained from Gaussian fits; 1σ statistical errors from the fit listed as uncertainties. As shown in Fig. 5, H99α lines were also detected toward G34.26+0.15 and G45.12+0.13, however, it was not possible to subtract the baseline as the lines were very board with respect to the bandpass, thus, line parameters were not reliably measured. In the case of G34.26+0.15, Sewilo et al. (2004) showed that the broad RRL profile is the convolution of multiple velocity components. Line parameters of G45.12+0.13 RRLs are reported in Araya et al. (2002) and Wood & Churchwell (1989).

Table 8. Other detections and tentative detections.

Source	Molecule[a]	Frequency (MHz)	Rms (mJy)	S_ν (Jy)	V_{LSR} (km s^{-1})	Width (km s^{-1})	$\int S_\nu d\nu$ (Jy km s^{-1})
IRAS 18566+0408 (?)	CH_3OH	6853.6870	5.0	0.017	83.27(0.07)	0.6(0.2)	0.004
IRAS 18566+0408 (?)	CH_3OH	7283.4490	4.6	0.021	90.41(0.06)	0.4(0.2)	0.003
			4.6	0.019	91.98(0.06)	0.1(0.2)	0.005
IRAS 18566+0408 (?)	CH	7348.4190	5.5	0.020	88.74(0.06)	0.4(0.2)	0.004
G45.12+0.13[b, c]	OH	6016.7460	2.5	− 0.026	55.8(0.2)	7.8(0.4)	− 0.214
G45.12+0.13[b, c, d]	OH	6030.7485	6.3	− 0.029	52.4(0.1)	1.9(0.3)	− 0.059
[b]			6.3	0.214	53.90(0.08)	2.0(0.2)	0.245
[b, c, d]			6.3	− 0.100	57.89(0.03)	4.32(0.08)	− 0.460

Notes. Tentative detections are marked with question marks (?).
[a]We also detected a line of thioformaldehyde (H_2CS) at 6.279 GHz toward G34.26+0.15 [S_ν = 16(1) mJy, V_{LSR} = 62.6(0.2) km s^{-1}, FWHM = 3.9(0.4) km s^{-1}; parameters from a Gaussian fit]; a discussion of this detection including follow-up observations will be the topic of a future article.
[b]2014 March observations, see Table 3.
[c]Line parameters from Gaussian fit. FWHM reported as line width.
[d]Two absorption lines fitted with independent Gaussians, however, it is likely that the absorption is a single broad line blended with masers.

lines observed in this project is listed in Tables 2–4. Table 5 lists the line parameters of the nine sources with detection of CH_3OH lines at 6.7 GHz. IRAS 18517+0437 shows the highest 6.7 GHz CH_3OH maser flux density (212 Jy); the weakest 6.7 GHz CH_3OH line was detected toward IRAS 19012+0536 (20 mJy); and the strongest absorption was found toward G34.26+0.15 (−318 mJy). Table 6 lists detections of the 6.035 GHz OH line toward five high-mass star-forming regions. The highest flux density was 7.51 Jy toward G45.47+0.05 and the strongest absorption was −129 mJy toward G45.12+0.13. The H99α line parameters are listed in Table 7. Table 8 shows other detections and tentative detections. Three tentative lines were found toward IRAS 18566+0408: 6.854 GHz CH_3OH, 7.283 GHz CH_3OH and 7.348 GHz CH; however, these lines were not confirmed in our follow-up observations (Table 3). It is unclear whether the tentative detections are variable lines or artefacts (see discussion in Section 4.3).

In Tables 5, 6, and 8 we list the peak channel flux density, peak channel velocity (channel width listed as uncertainty), linewidth above 3σ[4] (2 times the channel width listed as uncertainty), and integrated flux density. In a few cases where the lines were broad and approximately symmetric, the line parameters were instead obtained from Gaussian fits as indicated in table notes. The spectra of the detections and tentative detections are presented in Figs 1–6. To facilitate the use of our data, we also provide as Supporting Information the ASCII files used to generate the figures.

A potential problem in a targeted high-sensitivity survey such as ours is the possibility of sources at the edge of the primary beam and/or contamination by unrelated sources outside of the primary beam, that is spurious detections of nearby bright sources in the sidelobes. As pointed out by Breen et al. (2015), such contamination is possible in the case of weak lines detected with Arecibo. A source in our sample that could suffer from such contamination is the 6.7 GHz CH_3OH maser in G45.12+0.13 (Fig. 2), as we detected a strong maser toward the source G45.07+0.13 (Table 5 and Fig. 1) at the same peak velocity (57.83 ± 0.07 km s^{-1} for G45.07+0.13 versus 57.89 ± 0.07 km s^{-1} for G45.12+0.13). The angular separation between G45.07+0.13 and G45.12+0.13 is 3 arcmin, which is significantly greater than the HPBW of the telescope at 6.6 GHz (∼43 arcsec) as well as greater than the location of the first sidelobe of the telescope (∼1.2 arcmin; see beam pattern in Pandian et al. 2007). However, the flux density ratio between the strong maser in G45.07+0.13 and the weak maser in G45.12+0.13 is quite large (∼700), and thus, we cannot rule out contamination from a higher order sidelobe. A cross scan with the Arecibo Telescope or interferometric observations are needed to clarify the nature of the weak emission line toward G45.12+0.13.

Contamination by bright 6.7 GHz CH_3OH masers outside the primary beam for the other sources in our sample seems unlikely, as we found very similar spectral profiles for the other sources in common with the Methanol MultiBeam (MMB) survey (Breen et al. 2015). Also, previous interferometric observations of some of the sources show very similar spectral profiles to those reported here (e.g. Xu et al. 2009; Araya et al. 2010; Pandian et al. 2011). However, we emphasize that cross-scans and/or interferometric observations are needed to completely rule out contamination in the case of weak lines.

4 DISCUSSION

4.1 6.7 GHz CH_3OH absorption

4.1.1 Detections reported in this work

Figs 1 and 2 show our detection of 6.7 GHz methanol lines in nine star-forming regions. Among the sources in the sample, G34.26+0.15 is a well-known region of high-mass star formation that harbours methanol masers as well as absorption. The absorption line is also visible in the spectrum reported by Breen et al. (2015). The case of G34.26+0.15 exemplifies the challenges in detecting 6.7 GHz CH_3OH absorption, as strong masers coincident in velocity could easily mask weak absorption lines (e.g. Fig. 1a) and high-sensitivity observations are needed for detection. For example, Codella & Moscadelli (2000) studied the 6.7 GHz methanol masers toward the UCHII region in G34.26+0.15, but the typical rms of their observations was ∼3.5 Jy, which was too high for detection of the absorption line. G45.47+0.05 is another example where the rms of previous observations was too high for the detection of weak

[4]In case of overlapping lines, the linewidth above 3σ is measured up to the local minimum of the overlapping lines. For example, if two lines overlap, two linewidths are reported, one from the first channel above 3σ to the local minimum of the overlapping lines, and the other linewidth from the local minimum to the last channel above 3σ of the second line.

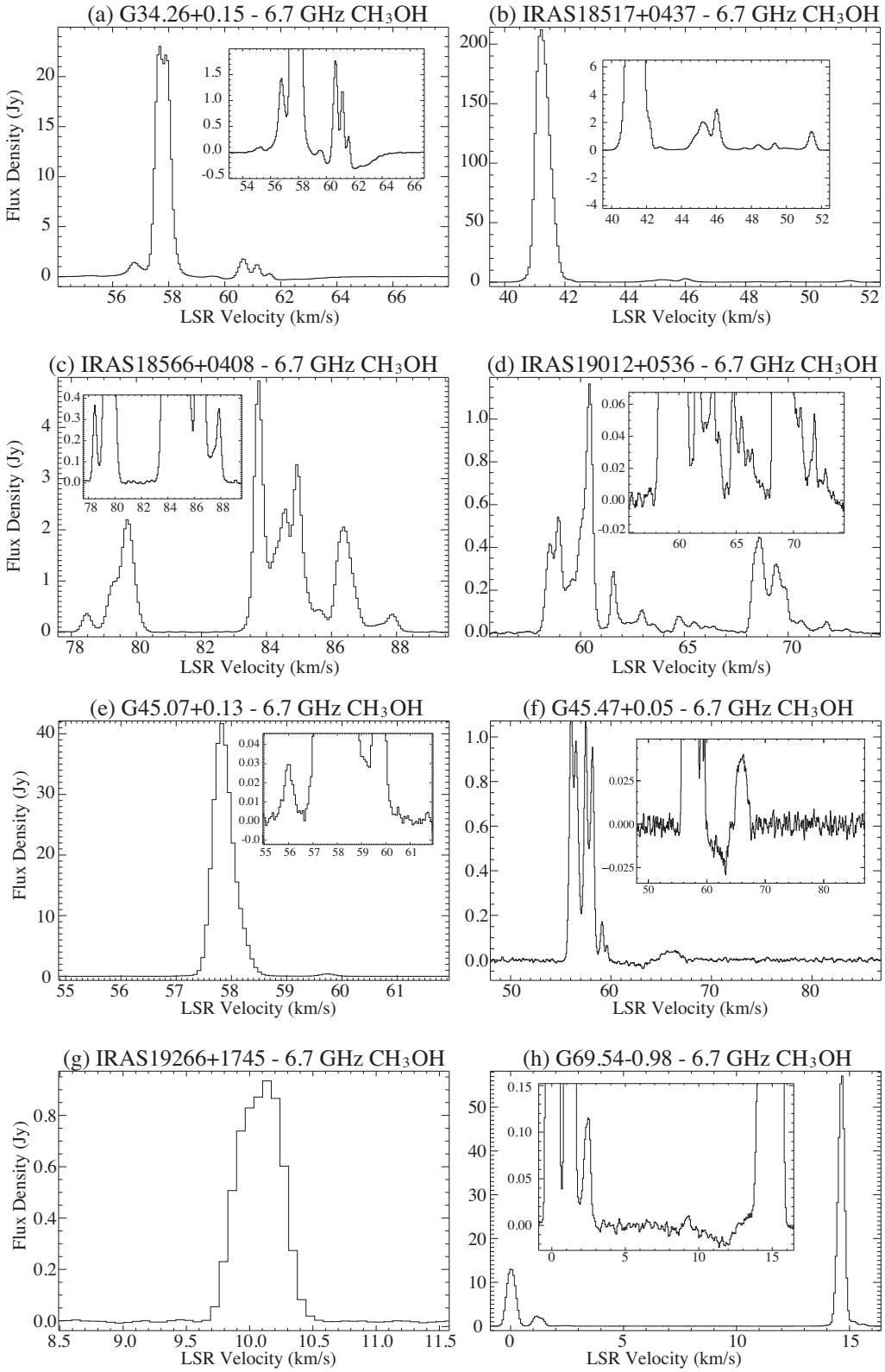

Figure 1. Detection of CH_3OH lines toward eight sources (see Table 5; the G45.12+0.13 spectra is shown in Fig. 2). Insets highlight weak masers and/or absorption. The data shown in the figure are available as Supporting Information.

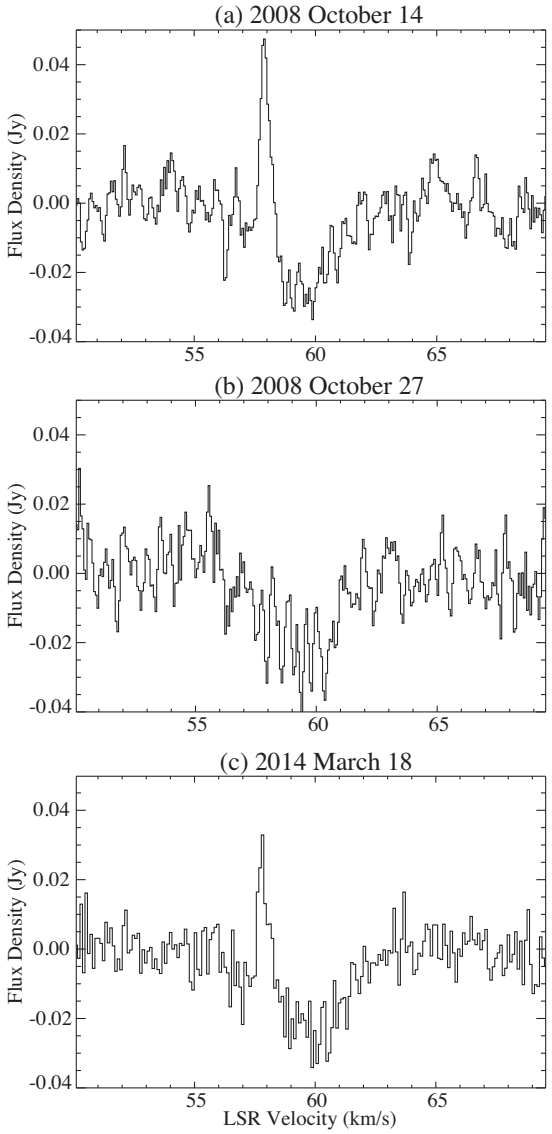

Figure 2. CH_3OH spectra of the 6.7 GHz transition toward G45.12+0.13 obtained in three epochs: (a) 2008 October 14; (b) 2008 October 27; and (c) 2014 March 18. Note the detection of a variable recurrent maser; as explained in Section 3, the line could be caused by detection of the strong maser in G45.07+0.13 in a sidelobe of the telescope. The data shown in the figure are available as Supporting Information.

absorption; Caswell et al. (1995) and Pandian et al. (2007) reported masers in this region with a typical rms of ∼60 and ∼70 mJy, respectively, which would render undetectable the −30 mJy line reported here.

To explore the physical conditions of the molecular clouds with 6.7 GHz absorption in our sample (Table 5), we focus on G45.12+0.13, as it is the only region whose absorption profile was not affected by overlapping maser lines in at least one epoch (Fig. 2). G45.12+0.13 harbours a cometary UCHII region (∼6 arcsec mean diameter, Wood & Churchwell 1989) against which NH_3 has been detected in absorption (Hofner et al. 1999). Our data show consistent 6.7 GHz absorption in three different epochs (see Fig. 2). We can rule out absorption solely against the CMB (e.g. from molecular material behind or to the side of the UCHII region but still within the Arecibo beam) based on the size of the Arecibo primary beam and the flux density of the absorption, because there would not be enough CMB flux density to account for the absorption if the cloud were smaller than the Arecibo beam, and an anti-inverted 6.7 GHz CH_3OH absorption region more extended than the Arecibo beam (behind the UCHII region) would be unreasonable based on the physical size of the region and physical conditions needed for anti-inversion (Impellizzeri et al. 2008). Thus, the absorption is most likely against the radio continuum of the UCHII region. In the case of local thermodynamic equilibrium (LTE), we obtain a CH_3OH column density of 10^{15} cm^{-2} assuming $T_K = 20$ K (e.g. Houghton & Whiteoak 1995) and a filling factor of 1[5] with respect to the continuum measured with Arecibo (Table 5). Similar column densities are likely for the other 6.7 GHz CH_3OH absorption regions in our sample, however significant overlap with maser lines precludes a reliable determination (see Fig. 1). The LTE analysis of 6.7 GHz CH_3OH absorption in Sgr B2 (Houghton & Whiteoak 1995) resulted in a CH_3OH column density of 10^{18} cm^{-2}, which is significantly greater than the column density we find for G45.12+0.13. Sgr B2 is one of the most extreme sites of star formation in our Galaxy, thus, a greater column density is reasonable.

4.1.2 Association with high-mass star-forming regions

Most 6.7 GHz CH_3OH studies focus on masers, whereas statistical studies of Galactic 6.7 GHz CH_3OH absorption have not been reported. We conducted an extensive literature review of 6.7 GHz CH_3OH surveys to search for absorption features, which may have been discussed in articles, included in tables, or simply shown in published maser spectra without discussion.[6] Table 9 shows the results of our literature review. We focus on blind surveys and/or high-sensitivity observations, and not on the large number of low-sensitivity and/or interferometric observations of 6.7 GHz CH_3OH masers that were unlikely to detect absorption (e.g. the single-dish surveys by Szymczak, Hrynek & Kus 2000 and Szymczak et al. 2002 had 3σ detection limits greater than 1 Jy). Also, while there are high-sensitivity blind interferometric surveys for CH_3OH masers (e.g. Rickert, Yusef-Zadeh & Ott 2019), high angular resolution observations with extended arrays can resolve out extended absorption, which would not be observable in maser spectra. We also exclude from Table 9 articles that focus on high-sensitivity studies of single prominent sources, as the detection rates from such studies would not be statistically meaningful. For instance, Houghton & Whiteoak (1995) were not included in Table 9 as they conducted an interferometric study of 6.7 GHz CH_3OH emission and absorption of Sgr B2, which had previously been detected in surveys. Likewise, we do not include in the table the extreme high-sensitivity observations with the Arecibo Telescope (0.2 mJy rms) of Arp 220, which resulted in detection of 6.7 GHz CH_3OH absorption (Salter et al. 2008). However, both sources (Sgr B2 and Arp 220) are included in Figs 7 and 8.

The detection rate of methanol absorption in our survey is 33 per cent, which, with the caveat of our relatively small sample, is among the highest detection rates found in the literature (most surveys have detection rates < 10 per cent).[7] We note that the papers

[5] A filling factor of 1 is assumed given that the absorption has not been imaged.
[6] An initial literature review of 6.7 GHz CH_3OH absorption was included in the MS thesis of Kim (2014).
[7] We stress that many of the detection rates listed in Table 9 were not explicitly reported in the articles but calculated based on spectra shown in the papers, thus, the detection rates should be considered lower limits as it is possible

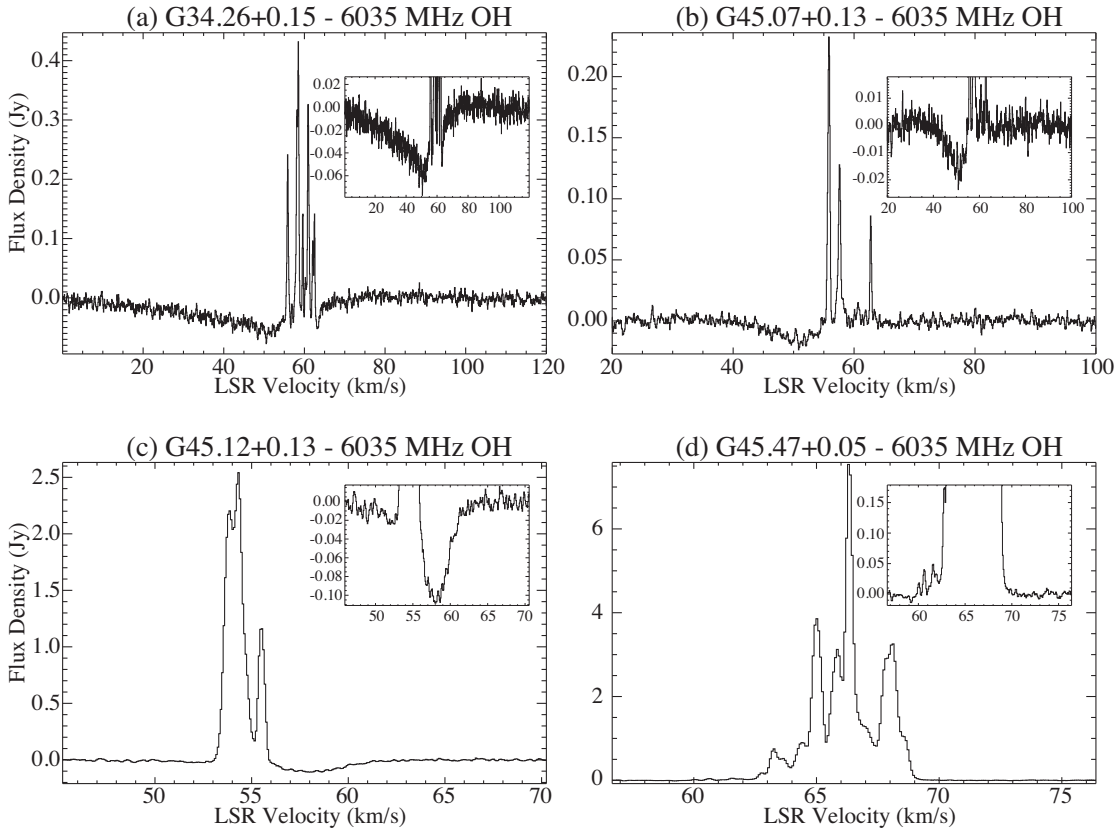

Figure 3. Detection of excited OH lines at 6.035 GHz toward four sources (see Table 6). Emission lines were detected in all cases; absorption was also found toward three regions. The inset panels show zoom-in views of the spectral lines. The data shown in the figure are available as Supporting Information.

with the highest absorption detection rates (Pandian et al. 2008; this work) were conducted with the 305-m Arecibo Telescope, which is the most sensitive telescope for detection of spectral lines at 6 GHz wavelengths. With the exception of the Effelsberg survey for extragalactic 6.7 GHz CH_3OH by Impellizzeri et al. (2008, which had an rms sensitivity between 0.6 and 8 mJy; see also Impellizzeri 2008), these surveys have among the lowest rms noise levels, and thus are most suitable to detect weak absorption features.

A graphical summary of the literature review is presented in Figs 7 and 8. Both panels of Fig. 7 show histograms of number of sources with 6.7 GHz methanol absorption for different bins of flux density absorption. In the upper panel, colours and line styles represent different ranges of compact radio continuum, that is flux density values from compact sources (no CMB or extended Galactic emission) in the telescope beam of the CH_3OH absorption features. The continuum values are from Table 5, Purcell et al. (2013), Hoare et al. (2012), Caswell & Haynes (1987) or interferometric observations from the NRAO VLA Image Archive.[8] Most sources where 6.7 GHz absorption lines have been reported harbour bright continuum sources, that is Fig. 7 (upper panel) is mostly populated by sources highlighted in green (thick solid line) and blue (thick dashed line) colours, that is sources with radio continuum greater than 0.1 Jy). Interferometric observations are needed to confirm that the absorption is against the compact radio continuum sources, as previously observed toward Sgr B2 (Houghton & Whiteoak 1995).

The lower panel of Fig. 7 examines the distribution of 6.7 GHz methanol absorption flux density for different full width at half-maximum (FWHM) values of the absorption lines. In some cases, the FWHM could not be measured due to overlapping bright masers. FWHM values less than 1.5 km s^{-1} could indicate relatively quiescent molecular environments, for example pre-stellar cores candidates, while values greater than 1.5 km s^{-1} indicate significant turbulent environments and/or outflows, for example regions of active star formation (e.g. Bergin & Tafalla 2007). No *bona fide* detections of narrow absorption lines ($<$1.5 km s^{-1}) were found in our literature review. For instance, G338.47+0.29 has the narrowest methanol absorption-like feature we found in the literature (FWHM $\sim$1 km s^{-1}, Gaylard & MacLeod 1993), however, the absorption was not detected in MMB data (Caswell et al. 2011), hence, the line was likely an artefact. Thus, the absorption lines in our literature review are broad, and taking into account the likely association with compact radio continuum sources, our study suggests that 6.7 GHz methanol absorption is tracing relatively evolved regions of high-mass star formation, that is in the UCHII region phase.

Fig. 8 shows absorption luminosity density ($L_{S_\nu} = 4\pi|S_{\nu,\mathrm{line}}|d^2$) as a function of FIR luminosity (estimated from *Herschel* data, Molinari et al. 2016) and radio luminosity density (from interfer-

that authors may have detected absorption lines but not shown them in spectra and/or not mentioned them in tables or text.

[8]We note that multiple continuum sources could be within the beam of the telescope used for detection of 6.7 GHz CH_3OH absorption; for example there is a compact, UC, and two hypercompact H II regions in the Arecibo beam of the G34.26+0.15 observations (e.g. Sewilo et al. 2004; Gómez et al. 2000).

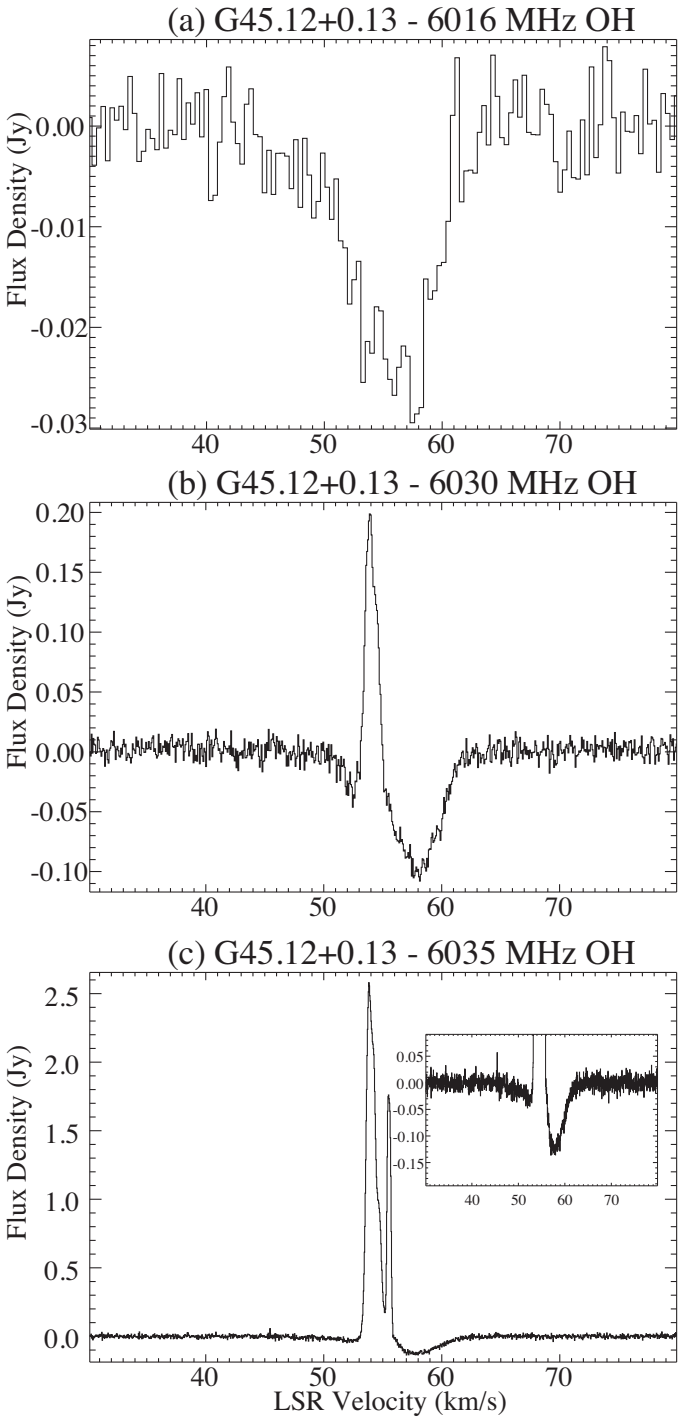

Figure 4. Detection of excited OH lines toward G45.12+0.13 at three different frequencies (see Tables 3, 6, and 8). The inset in the bottom panel shows a zoom-in view of the absorption line. The data shown in the figure are available as Supporting Information.

ometric observations). Our compilation of 6.7 GHz CH_3OH absorption regions show a weak dependence of absorption flux density with IR luminosity for Galactic sources (i.e. excluding NGC 3079, Arp 220, and Mrk 348), and a stronger dependence of line absorption with radio continuum luminosity, which again supports the interpretation that the absorption is associated with compact ionized regions instead of absorption against extended Galactic and CMB continuum.

A selection bias is a concern as many surveys (including this one) were targeted observations toward active regions of star formation, hence, association with star formation is expected. Blind maser surveys can easily miss absorption toward weak radio continuum sources (such as low-mass star-forming regions) because their sensitivity is appropriate for much stronger features. For instance, Pandian et al. (2007) conducted a blind survey with the Arecibo Telescope and absorption was found only toward one region of

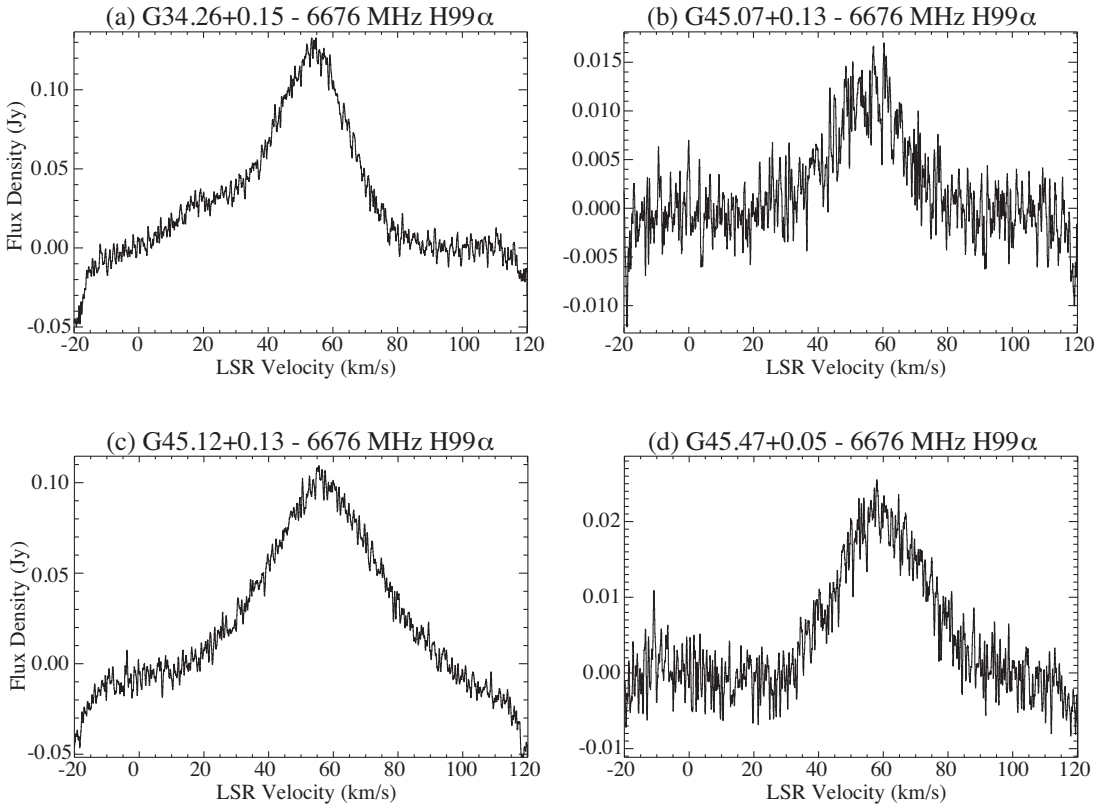

Figure 5. Detection of the H99α radio recombination line at 6.676 GHz toward four sources. In the case of G34.26+0.15 and G45.12+0.13, the line parameters could not be reliably measured (see Table 7). The data shown in the figure are available as Supporting Information.

high-mass star formation; their rms (70–85 mJy) was too high to detect weak absorption features in low-mass star-forming regions, such as those reported by Pandian et al. (2008). Another large-scale blind survey of this transition is the 6.7 GHz MMB project (Caswell et al. 2010, 2011; Green et al. 2010, 2012; Breen et al. 2015), which searched for bright methanol masers across the Galactic plane. The typical rms of the MMB main survey is $\sim$0.17 Jy and the rms of the MMB MX follow-ups is $\sim$0.07 Jy, for example Caswell et al. (2010), which precludes detection of weak absorption features.

The work by Olmi et al. (2014) shows that despite the observational bias, our conclusion that 6.7 GHz CH_3OH absorption is tracing mostly regions with compact radio continuum sources, that is active sites of high-mass star formation, is reliable. They observed 107 Herschel infrared GALactic Plane Survey (Hi-GAL) sources with the Arecibo Telescope with high sensitivity ($\sim$5–10 mJy rms) but found only *one* possible absorption feature in G59.78+0.63 (see their figure 3). Olmi et al. (2014) do not report radio continuum data toward the observed methanol masers, however, the authors carried out follow-up VLA observations of a smaller sample of sources, that allowed them to map the compact radio emission (Olmi et al., in preparation). They found that in most cases the peak flux density was $\lesssim$ 1 mJy beam^{-1} (in one case it was as high as $\sim$26 mJy beam^{-1}). Thus, the combination of high-sensitivity, low radio continuum, and low detection rate supports our conclusion that 6.7 GHz CH_3OH absorption mostly traces active star-forming regions with significant free–free emission, instead of cold molecular clouds with absorption against the CMB.

4.2 Excited OH lines

Another transition included in our survey is the 6.035 GHz OH line, which has been found in other high-mass star-forming regions (e.g. Fish, Sjouwerman & Pihlström 2007). We detected 6.035 GHz OH masers in 5 of the 12 regions (one is a very weak detection toward IRAS 18566+0408), and absorption in three of the five sources. To our knowledge, the 6035 MHz OH masers toward G45.07+0.13 are a new detection. Although G45.07+0.13 was observed by Avison et al. (2016), their 3σ detection limit of about 0.5 Jy is higher than the $\sim$0.02 − 0.2 Jy flux densities that we measured. We list the rms and the line parameters of the detections in Table 6 (see also Figs 3, 4, and 6). Four of the regions have strong radio continuum (Table 6), as also confirmed by the detection of hydrogen radio recombination lines (Fig. 5); IRAS 18566+0408 has a weak radio continuum source ($\sim$1 mJy; Araya et al. 2005; Hofner et al. 2017). We discuss in more detail two of the sources here:

4.2.1 G34.26+0.15

Al-Marzouk et al. (2012) reported 6.035 GHz OH masers and a broad 6.035 GHz OH absorption feature in G34.26+0.15.[9] The observations reported here confirm this broad absorption. The absorption line is asymmetric, with a prominent low-velocity wing indicative of

[9]The masers in this source were also detected by Avison et al. (2016) at similar flux density levels, but the absorption line was below their sensitivity level.

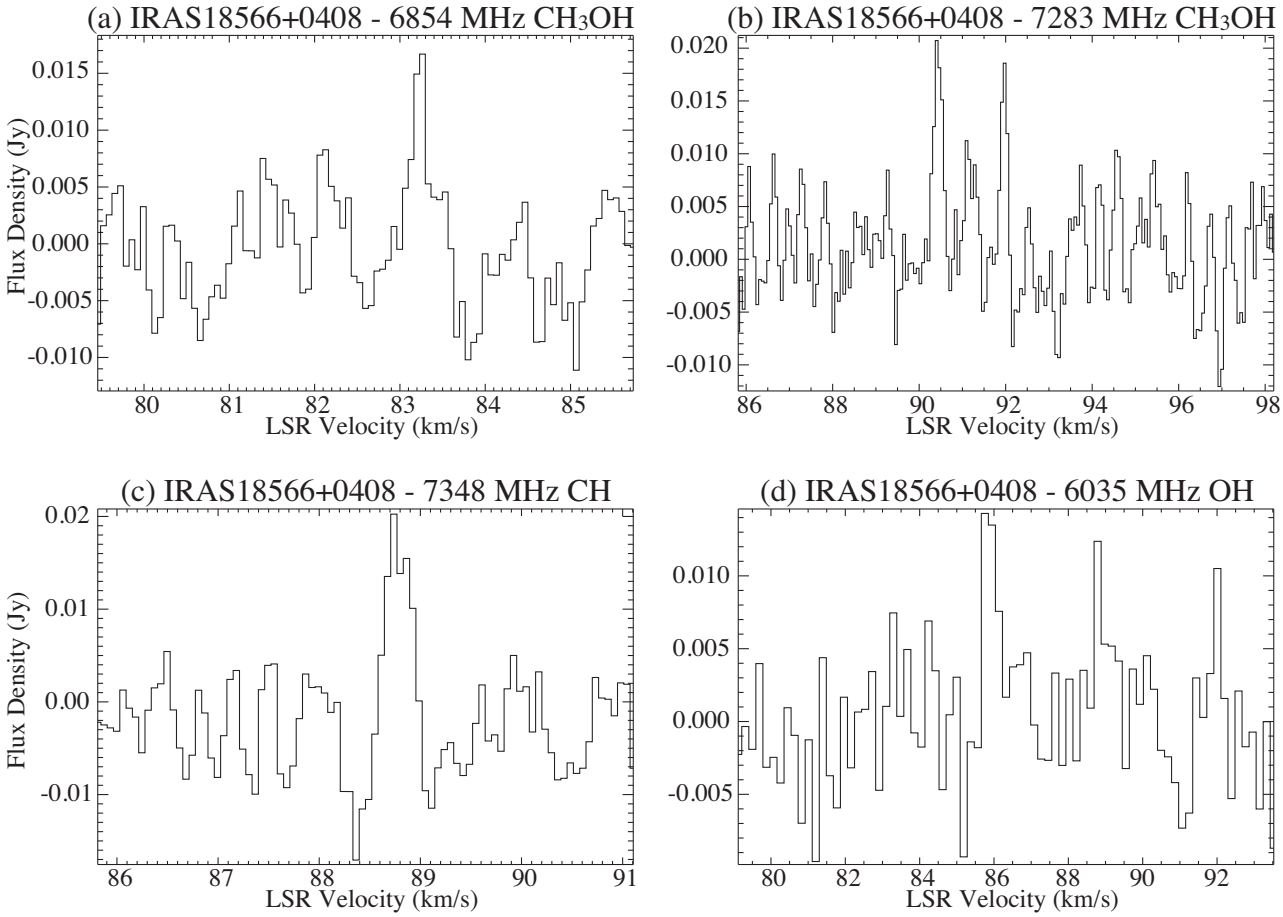

Figure 6. Spectra of weak lines toward IRAS 18566+0408. Panels (a)–(c) show tentative detections, while the weak line shown in panel (d) is a confirmed 6.035 GHz OH detection, as Al-Marzouk et al. (2012) reported this line and showed that the line is highly variable, possibly correlated with the variability of 6.7 GHz CH_3OH masers in the region. The tentative detections were not confirmed in the follow-up observations (Table 3), thus the lines may be variable or artefacts. The data shown in the figure are available as Supporting Information.

outflow/expansion motion (see Fig. 3)[10]; possibly associated with the CO outflow reported by Yang et al. (2018). The G34.26+0.15 region shows strong infall signatures in many common molecular lines (e.g. Liu, Wu & Zhang 2013; Wyrowski et al. 2016) which affect and dilute potential traces of expanding motions. The OH signal we discovered clearly shows a blueshifted asymmetry indicating expansion and based on VLA observations (article in preparation), the absorption is in front of the cm continuum, which removes any geometric ambiguity when interpreting the line kinematics.

4.2.2 G45.12+0.13

In addition to the 6.035 GHz OH emission and absorption lines shown in Fig. 3, we detected OH lines at 6.016 GHz (absorption) and 6.030 GHz (absorption and emission) toward G45.12+0.13 (Fig. 4). The figure also includes a second epoch of the 6.035 GHz OH transition: the spectra from Fig. 3 show data from 2008, while Fig. 4 shows data from 2014 March. It is evident from the figures that the 6.035 GHz absorption profile is consistent between both epochs, but some changes are clear in the maser profile. In particular, the disappearing of the double peak of the brightest maser between 53 and 55 km s^{-1} (although the line from 2014 March, Fig. 4, shows a red asymmetry indicative of overlapping masers). There is also an increase in intensity of the high-velocity maser peak at 55.5 km s^{-1}. Variability of the maser profile is also evident when comparing to the spectrum reported by Avison et al. (2016).

We detected OH absorption in the three observed 6 GHz OH transitions, with the 6.016 GHz OH line being the weakest. The 6.016, 6.030, and 6.035 GHz absorption lines are detected at the same velocity, near 58 km s^{-1} (Fig. 4). As in the case of OH absorption lines detected toward Sgr A East (Fish et al. 2007), the 6 GHz lines in G45.12+0.13 likely trace thermal absorption against the radio continuum source. Masers were detected at 6.030 and 6.035 GHz at a velocity of ∼55 km s^{-1}, but we did not detect emission of the 6.016 GHz line at a 3σ level of 7.5 mJy. Detection of masers at 6.030 and 6.035 GHz, with the 6.035 GHz maser being brighter, and no detection of a 6.016 GHz maser, is expected from theoretical models of OH masers in star-forming regions (Cragg, Sobolev & Godfrey 2002).

4.3 Tentative detections and non-detections

Fig. 6 shows spectra of weak lines tentatively detected toward the high-mass star-forming region IRAS 18566+0408, but not confirmed

[10]Additional observations of the absorption line were presented in the MS thesis of Kim (2014).

Table 9. Literature review of 6.7 GHz methanol absorption.

Reference	Telescope	Beam size (arcsec)	Rms[a] (mJy)	Total number of targets[b]	Absorption[c]	Emission	Abs. detection rate (per cent)[d]
This work	Arecibo	43	5	12	4	9	33
Breen et al. (2015)[e]	Parkes	192	70	(265)	5	265	2
Caswell et al. (1995)	Parkes	192	60	245	11	245	4
Caswell et al. (2010)[e]	Parkes	192	70	(183)	5	183	3
Caswell et al. (2011)[e]	Parkes	192	70	(198)	4	198	2
Fontani, Cesaroni & Furuya (2010)	Effelsberg	120	50	296	0	55	0
Gaylard & MacLeod (1993)	Hartebeesthoek	420	500	62	2?[f]	18	3
Green et al. (2010)[e]	Parkes	192	70	(119)	2	119	2
Green et al. (2012)[e]	Parkes	192	70	(207)	6	207	3
Impellizzeri et al. (2008)	Effelsberg	120	0.6–8	8	1	0	13
Impellizzeri (2008)	Effelsberg	120	0.6–12	10	2?[g]	2?[g]	20
Menten (1991)	140ft NRAO	300	400	123	8	80	7
Olmi et al. (2014)	Arecibo	43	5	107	1	37	1
Pandian et al. (2007)	Arecibo	43	70	(86)	1	86	1
Pandian et al. (2008)	Arecibo	43	1.2	5	2	0	40
Walsh et al. (1997)	Parkes	198	100	535	3	201	0.6
Xu et al. (2008)	Effelsberg	120	100	89	1	10	1
Yang et al. (2017)	TMRT	180	20	1473	0	12	0

Notes. [a] Representative rms values from the articles are listed. We give a range in cases where rms values for different sources varied by a factor of ∼10 or more.
[b] The column lists the total number of sources observed in a specific survey including non-detections. In case of blind surveys, we list in parenthesis the number of sources with 6.7 GHz CH_3OH detection (emission and/or absorption).
[c] In many cases, the number of regions with absorption reported in the table should be considered a lower limit, as the presence of absorption was based on inspection of published spectra designed to show masers and not weak absorption features; in addition, not all spectra were shown in the articles (e.g. Walsh et al. 1995, 1997; Xu et al. 2008; Yang et al. 2017).
[d] The detection rate in the case of blind surveys is the percentage of sources detected (emission or absorption) that show absorption.
[e] Part of the MMB Survey (Green et al. 2009). In most cases, spectra shown in MMB papers are from Parkes MX-mode follow-up observations (∼70 mJy rms) instead from the main survey cubes (∼170 Jy rms); for example, see Caswell et al. (2010).
[f] Gaylard & MacLeod (1993) reported absorption toward G338.47+0.29, however, the absorption was not detected in MMB data (Caswell et al. 2011), hence, the absorption feature was likely an artefact.
[g] In addition to the detection of 6.7 GHz CH_3OH absorption toward NGC 3079, Mrk 348 was listed as a tentative detection. Tentative detection of 6.7 GHz CH_3OH emission was reported toward Mrk 3 and NGC 6240. We note that a subsample of the observations reported in Impellizzeri (2008) were published in Impellizzeri et al. (2008), that is these are not independent studies.

in our follow-up observations. Even though the lines are weak, at least the 6.035 GHz OH transition is a reliable detection, given that it is found at the same velocity as the 6.035 GHz OH maser reported by Al-Marzouk et al. (2012). As mentioned in that paper, this 6.035 GHz OH maser is variable, which would explain the low intensity detected in this project. The excited CH_3OH lines at 6.854 and 7.283 GHz and the CH line at 7.348 GHz are tentative detections as they have flux densities just above the 3σ level. Their local standard of rest (LSR) velocities compared with detections of other transitions (e.g. Araya et al. 2010) suggest that they are real, although as noted above, these lines were not confirmed in our follow-up observations (Table 3). Given the strong variability of several molecular maser species in IRAS 18566+0408 (Araya et al. 2010; Al-Marzouk et al. 2012), it is possible that the tentative lines are variable masers, although further high-sensitivity observations are needed to confirm this. We note that theoretical work (Sobolev, Cragg & Godfrey 1997) predicts inversion of the 7.283 GHz CH_3OH transition. We found no reference to previous detections of these transitions in the literature, for example, see Matthews et al. (1986) for the case of CH.

As reported in Tables 2 and 3, other transitions of several species like D_2CO, CH_3CHO, and CH were not detected. These non-detections are not surprising because of abundance constraints, the need of extreme column densities, and/or special physical conditions needed for population inversion. Specifically, non-detections of D_2CO are expected as the abundance of double deuterated molecules is low (e.g. Turner 1990). In the case of CH_3CHO, detectable emission of the transition included in this work requires extreme environments (the transition has been only reported toward Sgr B2, Bell, Matthews & Feldman 1983; although other CH_3CHO transitions have been detected in other sources, see Matthews, Friberg & Irvine 1985; Ikeda et al. 2001; Chengalur & Kanekar 2003). Regarding the non-detections of other CH_3OH transitions, bright masers of these low-frequency lines require very special conditions for population inversion (e.g. Sobolev et al. 1997). In the case of the CH non-detections, the energy levels of the rotational-excited transitions included in this work are unlikely to be significantly populated (see non-detections reported by Matthews et al. 1986).

5 SUMMARY

We report one of the highest sensitivity surveys for molecular lines at 6 GHz frequencies conducted to date. The 305-m Arecibo Telescope was used to observe a sample of 12 intermediate- and high-mass star-forming regions. Molecular transitions of CH, CH_3CHO, CH_3C_5N, CH_3OH, D_2CO, H_2CS, OH, and radio recombination lines were searched for, with channel widths between 0.03 and 0.7 km s^{-1} and achieving rms levels of the order of ∼5 mJy for most sources and transitions. We confirmed broad absorption of the 6.035 GHz OH transition toward G34.26+0.15. The absorption is asymmetric and

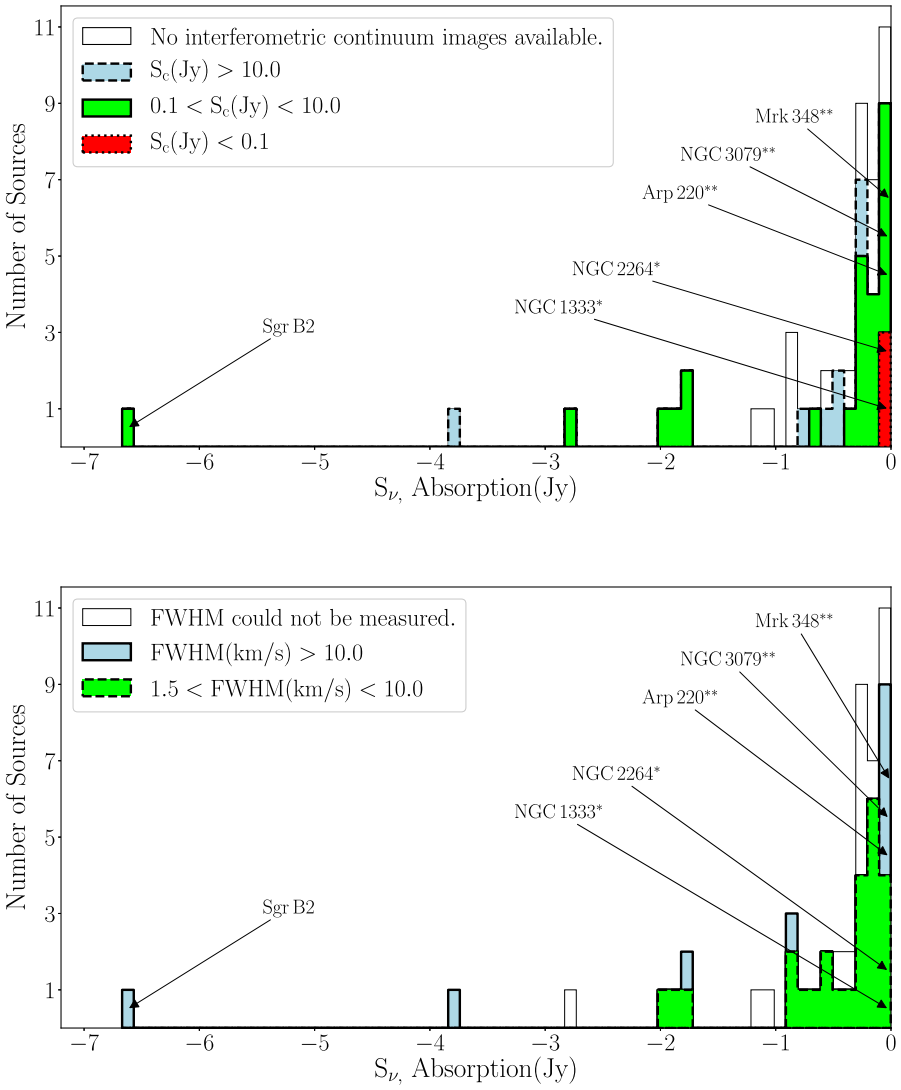

Figure 7. Histogram of the number of sources with 6.7 GHz methanol absorption at different flux density bins. Colours and line type (solid, dashed, and dotted) in the upper panel identify the radio continuum flux density based on interferometric images. Colours and line type in the lower panel identify ranges in FWHM of the absorption lines. (*) NGC 1333 is a low-mass star-forming region and the absorption is against the CMB (Pandian et al. 2008). The absorption line detected toward NGC 2264 is also likely against the CMB (Pandian et al. 2008). (**) Extragalactic absorption has been reported toward NGC 3079, Arp 220, and Mrk 348.

shows a blueshifted velocity wing indicative of expansion (perhaps an outflow) of molecular material.

Our high-sensitivity observations allowed us to investigate an aspect of the 6.7 GHz CH_3OH transition that has been often neglected in the literature, that is absorption. We report detection of absorption in four regions of our sample, that is a 33 per cent detection rate, which is among the highest detection rates of 6.7 GHz CH_3OH absorption reported in the literature. A literature review of 6.7 GHz CH_3OH absorption shows that the known absorption sources are mostly high-mass star-forming regions with bright (>0.1 Jy) continuum sources.

ACKNOWLEDGEMENTS

We acknowledge an anonymous referee for comments that greatly improved our manuscript. EDA acknowledges partial support from the National Science Foundation (NSF) grant AST-1814063, a Summer Stipend Grant from Western Illinois University, and computational resources donated by the WIU Distinguished Alumnus Frank Rodeffer. PH acknowledges partial support from NSF grant AST-1814011. EDA would like to thank WIU AstroLab students for participating in the project, in particular Daniel M. Halbe and Hyung Kwan Kim; also José Andrés Díaz Loría for taking part in the planning stages of one of the telescope proposals. The Arecibo Observatory is operated by the University of Central Florida under a cooperative agreement with the National Science Foundation (AST-1822073), and in alliance with Universidad Ana G. Méndez and Yang Enterprises. This research has made use of NASA's Astrophysics Data System. The NRAO is a facility of the National Science Foundation operated under cooperative agreement by Associated Universities, Inc.

DATA AVAILABILITY

The data underlying this article are available in the article and in its online Supporting Information.

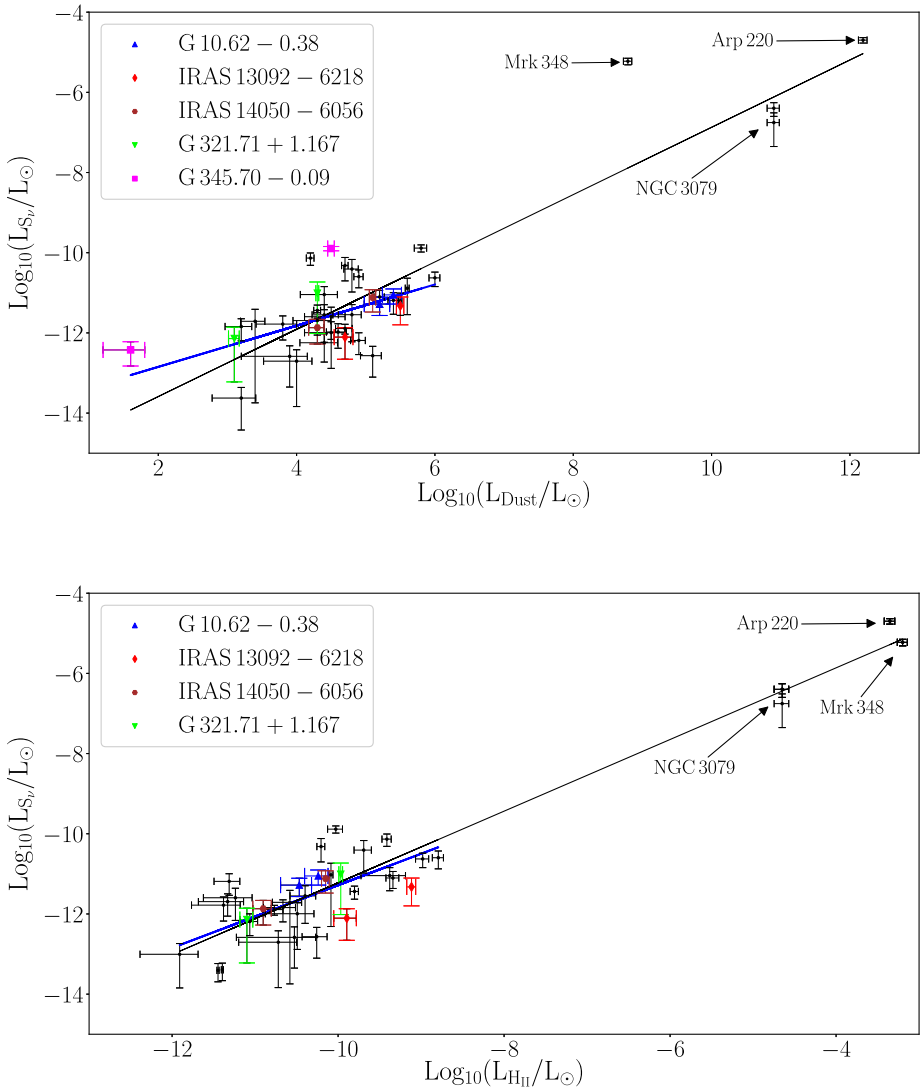

Figure 8. Absorption luminosity of the 6.7 GHz CH_3OH line ($L_{S_\nu} = 4\pi|S_{\nu,\mathrm{line}}|d^2$) as a function of FIR luminosity (upper panel) and 5 GHz radio luminosity (lower panel). Sources identified with different symbols and colours are regions for which the distance ambiguity has not been resolved, and thus, significantly different luminosity values are possible. No interferometric continuum observations of G345.70−0.09 are available, thus, it was not included in the lower panel. All data in the upper panel were fit with an $\alpha = 0.84 \pm 0.07$ power law (black fit); and the thick slope (blue line) shows the fit ($\alpha = 0.51 \pm 0.14$) when the extragalactic sources are excluded. The data in the lower panel were also fit with a power law ($\alpha = 0.89 \pm 0.05$) when all data are included (black fit), and with a power-law $\alpha = 0.78 \pm 0.16$ when only sources with $\log(L_{\mathrm{HII}}/L_\odot)$ between −12 and −8 are included (thick fit line shown in blue).

REFERENCES

Al-Marzouk A. A., Araya E. D., Hofner P., Kurtz S., Linz H., Olmi L., 2012, ApJ, 750, 170
Araya E., Hofner P., Churchwell E., Kurtz S., 2002, ApJS, 138, 63
Araya E., Hofner P., Linz H., Sewilo M., Watson C., Churchwell E., Olmi L., Kurtz S., 2004, ApJS, 154, 579
Araya E., Hofner P., Kurtz S., Linz H., Olmi L., Sewilo M., Watson C., Churchwell E., 2005, ApJ, 618, 339
Araya E., Hofner P., Olmi L., Kurtz S., Linz H., 2006, AJ, 132, 1851
Araya E., Hofner P., Kurtz S., Olmi L., Linz H., 2008, ApJ, 675, 420
Araya E. D., Hofner P., Goss W. M., Kurtz S., Richards A. M. S., Linz H., Olmi L., Sewiło M., 2010, ApJ, 717, L133
Avison A. et al., 2016, MNRAS, 461, 136
Bell M. B., Matthews H. E., Feldman P. A., 1983, A&A, 127, 420
Bergin E. A., Tafalla M., 2007, ARA&A, 45, 339
Beuther H., Schilke P., Menten K. M., 2002, ApJ, 566, 945
Breen S. L. et al., 2015, MNRAS, 450, 4109
Caswell J. L., Haynes R. F., 1987, A&A, 171, 261
Caswell J. L., Vaile R. A., Ellingsen S. P., Whiteoak J. B., Norris R. P., 1995, MNRAS, 272, 96
Caswell J. L. et al., 2010, MNRAS, 404, 1029
Caswell J. L. et al., 2011, MNRAS, 417, 1964
Cesaroni R. et al., 2015, A&A, 579, A71
Chengalur J. N., Kanekar N., 2003, A&A, 403, L43
Codella C., Moscadelli L., 2000, A&A, 362, 723
Cragg D. M., Sobolev A. M., Godfrey P. D., 2002, MNRAS, 331, 521
Ellingsen S. P., Norris R. P., Whiteoak J. B., Vaile R. A., McCulloch P. M., Price M. G., 1994, MNRAS, 267, 510
Fish V. L., Sjouwerman L. O., Pihlström Y. M., 2007, ApJ, 670, L117
Fontani F., Cesaroni R., Furuya R. S., 2010, A&A, 517, A56
Gaylard M. J., MacLeod G. C., 1993, MNRAS, 262, 43

Goedhart S., Gaylard M. J., van der Walt D. J., 2004, MNRAS, 355, 553
Gómez Y., Rodríguez-Rico C. A., Rodríguez L. F., Garay G., 2000, Rev. Mex. Astron. Astrofis., 36, 161
Green J. A. et al., 2009, MNRAS, 392, 783
Green J. A. et al., 2010, MNRAS, 409, 913
Green J. A., Caswell J. L., Fuller G. A., 2012, MNRAS, 420, 3108
Hoare M. G. et al., 2012, PASP, 124, 939
Hofner P. et al., 1999, ApJ, 514, 899
Hofner P., Cesaroni R., Kurtz S., Rosero V., Anderson C., Furuya R. S., Araya E. D., Molinari S., 2017, ApJ, 843, 99
Houghton S., Whiteoak J. B., 1995, MNRAS, 273, 1033
Ikeda M., Ohishi M., Nummelin A., Dickens J. E., Bergman P., Hjalmarson A., Irvine W. M., 2001, ApJ, 560, 792
Impellizzeri C. M. V., 2008, PhD thesis, University of Bonn
Impellizzeri C. M. V., Henkel C., Roy A. L., Menten K. M., 2008, A&A, 484, L43
Kim H. K., 2014, MS thesis, Western Illinois University
Kurtz S., Churchwell E., Wood D. O. S., 1994, ApJS, 91, 659
Kurtz S., Cesaroni R., Churchwell E., Hofner P., Walmsley C. M., 2000, Protostars and Planets IV. Univ. Arizona Press, Tucson, AZ, p. 299
Liu T., Wu Y., Zhang H., 2013, ApJ, 776, 29
MacLeod G. C. et al., 2018, MNRAS, 478, 1077
Matthews H. E., Friberg P., Irvine W. M., 1985, ApJ, 290, 609
Matthews H. E. et al., 1986, A&A, 161, 329
Menten K. M., 1991, ApJ, 380, L75
Miralles M. P., Rodriguez L. F., Scalise E., 1994, ApJS, 92, 173
Molinari S. et al., 2016, A&A, 591, A149
Olmi L., Araya E. D., Hofner P., Molinari S., Morales Ortiz J., Moscadelli L., Pestalozzi M., 2014, A&A, 566, A18
Pandian J. D., Goldsmith P. F., Deshpande A. A., 2007, ApJ, 656, 255
Pandian J. D., Leurini S., Menten K. M., Belloche A., Goldsmith P. F., 2008, A&A, 489, 1175
Pandian J. D., Momjian E., Xu Y., Menten K. M., Goldsmith P. F., 2011, ApJ, 730, 55
Peng R., Whiteoak J. B., 1991, PASA, 9, 287
Purcell C. R. et al., 2013, ApJS, 205, 1
Rajabi F., Houde M., Bartkiewicz A., Olech M., Szymczak M., Wolak P., 2019, MNRAS, 484, 1590
Rickert M., Yusef-Zadeh F., Ott J., 2019, MNRAS, 482, 5349
Rosero V. et al., 2016, ApJS, 227, 25
Salter C. J., Ghosh T., Catinella B., Lebron M., Lerner M. S., Minchin R. , Momjian E., 2008, AJ, 136, 389
Sewilo M., Churchwell E., Kurtz S., Goss W. M., Hofner P., 2004, ApJ, 605, 285
Sjouwerman L. O., Murray C. E., Pihlström Y. M., Fish V. L., Araya E. D., 2010, ApJ, 724, L158
Sobolev A. M., Cragg D. M., Godfrey P. D., 1997, MNRAS, 288, L39
Sridharan T. K., Beuther H., Schilke P., Menten K. M., Wyrowski F., 2002, ApJ, 566, 931
Strack A. et al., 2019, ApJ, 878, 90
Szymczak M., Hrynek G., Kus A. J., 2000, A&AS, 143, 269
Szymczak M., Kus A. J., Hrynek G., Kěpa A., Pazderski E., 2002, A&A, 392, 277
Szymczak M., Olech M., Sarniak R., Wolak P., Bartkiewicz A., 2018, MNRAS, 474, 219
Tan W. S., 2017, MS thesis, Western Illinois University
Turner B. E., 1990, ApJ, 362, L29
Walmsley C. M., Batrla W., Matthews H. E., Menten K. M., 1988, A&A, 197, 271
Walsh A. J., Lyland A. R., Robinson G., Bourke T. L., James S. D., 1995, PASA, 12, 186
Walsh A. J., Hyland A. R., Robinson G., Burton M. G., 1997, MNRAS, 291, 261
Watson C., Araya E., Sewilo M., Churchwell E., Hofner P., Kurtz S., 2003, ApJ, 587, 714
Williams S. J., Fuller G. A., Sridharan T. K., 2004, A&A, 417, 115
Wood D. O. S., Churchwell E., 1989, ApJS, 69, 831
Wyrowski F. et al., 2016, A&A, 585, A149
Xu Y., Li J. J., Hachisuka K., Pandian J. D., Menten K. M., Henkel C., 2008, A&A, 485, 729
Xu Y., Voronkov M. A., Pandian J. D., Li J. J., Sobolev A. M., Brunthaler A., Ritter B., Menten K. M., 2009, A&A, 507, 1117
Yang K. et al., 2017, ApJ, 846, 160
Yang A. Y., Thompson M. A., Urquhart J. S., Tian W. W., 2018, ApJS, 235, 3

SUPPORTING INFORMATION

Supplementary data are available at *MNRAS* online.

Figure S1. ASCII data used to generate Figure 1. Detection of CH_3OH lines toward eight sources (see Table 5; the G45.12+0.13 spectra is shown in Fig. 2).
Figure S2. ASCII data used to generate Figure 2. CH_3OH spectra of the 6.7 GHz transition toward G45.12+0.13 obtained in three epochs: (a) 2008 October 14; (b) 2008 October 27; and (c) 2014 March 18.
Figure S3. ASCII data used to generate Figure 3. Detection of excited OH lines at 6.035 GHz toward four sources (see Table 6).
Figure S4. ASCII data used to generate Figure 4. Detection of excited OH lines toward G45.12+0.13 at three different frequencies (see Tables 3, 6, and 8).
Figure S5. ASCII data used to generate Figure 5. Detection of the H99α radio recombination line at 6.676 GHz toward four sources.
Figure S6. ASCII data used to generate Figure 6. Spectra of weak lines toward IRAS 18566+0408.

Please note: Oxford University Press is not responsible for the content or functionality of any supporting materials supplied by the authors. Any queries (other than missing material) should be directed to the corresponding author for the article.

This paper has been typeset from a TEX/LATEX file prepared by the author.